

Topological Defects in Semiconducting Carbon Nanotubes as Triplet Exciton Traps and Single-Photon Emitters

Timur Biktagirov^{1*}, Uwe Gerstmann¹, Wolf Gero Schmidt¹

¹Universität Paderborn, Department Physik, Warburger Str. 100, 33098 Paderborn, Germany

*Timur.Biktagirov@upb.de

ABSTRACT: We investigate the role of topological defects in exciton behavior in (6,5) semiconducting single-walled carbon nanotubes using density functional theory. Our study identifies the helical Stone-Wales defect as a prominent trap for triplet excitons, characterized by a large zero-field splitting consistent with experimental data and a small singlet-triplet gap. The weak electron-phonon coupling, as evidenced by a Huang-Rhys factor of 0.74, renders it a promising single-photon emitter, with the zero-phonon line predicted at 1.6 μm , within the telecom range. These insights into defect-engineered electronic structure and exciton dynamics offer promising opportunities for improving the performance of carbon nanotube-based quantum light sources and optoelectronic devices.

KEYWORDS: *carbon nanotubes, quantum defects, excitons, photonics, first-principles calculations*

Semiconducting single-walled carbon nanotubes (SWCNTs) are quasi-one-dimensional materials with unique photonic functionalities [1] that can be exploited in optoelectronic devices [2–4], quantum-enhanced sensors [5, 6], and telecom-range single-photon emitters [7–9]. SWCNTs can now be produced with specific chiralities, enabling control over their electronic structures and optical responses [10, 11]. However, the details of their excited state dynamics, which are imperative for effective photophysical and quantum technological applications, remain a focus of active research.

Excitons (electron-hole pairs) in SWCNTs exhibit large binding energies [12] and very high mobility [13]. Therefore, if the nanotube walls contain structural defects, fast-diffusing free excitons are likely to be trapped at the defect-induced electronic states and localize at the defect site (see Figure 1A) [14]. It has been experimentally shown that intentional implantation of defects in semiconducting SWCNTs prevents free excitons from encountering recombination sites, which increases photoluminescence quantum yields [15–18].

Initially, a defect-trapped exciton (DTE) is formed in a singlet state ($S = 0$), but it can transition to a triplet state ($S = 1$) through a spin-forbidden process known as intersystem crossing (ISC) [19]. Photogenerated triplet states are of great interest because they can be directly detected by electron paramagnetic resonance (EPR) and related techniques, offering unique insights into the material's photophysics. Furthermore, typically long lifetimes and quantum coherence times of triplet excitons in organic materials make them pivotal to light-emitting devices [20] and promising spin qubit candidates [21]. Triplet excitons in semiconducting SWCNTs have been observed using transient absorption spectroscopy [22, 23] and optically detected magnetic resonance (ODMR) [24–27]. Notably, ODMR measurements of triplets in

(6,5) chirality SWCNTs reveal their definitive spectroscopic fingerprint, the zero-field splitting (ZFS) between the $m_s = 0$ and $m_s = \pm 1$ spin sublevels [25, 27]. ZFS arises from the magnetic dipolar interaction between the two unpaired electrons, reflecting their spatial distribution [28]. The substantial observed ZFS indicates well-localized triplet excitons in these nanotubes. Additionally, Ref. [27] identifies coexistence of at least two photoinduced triplets with distinct ZFS values (550 MHz and 150 MHz) and hints at a role for defects in forming these triplet states, even in nominally pristine nanotubes.

SWCNTs often contain topological defects (TDs), i.e., non-six-membered carbon rings, spontaneously created during synthesis, purification, or chemical processing [29, 30]. One of the most ubiquitous types of TDs is the Stone-Wales (SW) defect, formed by a 90-degree rotation of one C-C pair, resulting in two heptagons and two pentagons (5-7-7-5) [31]. Although these and many other TDs do not alter the nanotube's chirality and are challenging to detect experimentally, they can significantly impact the electronic structure and excitonic properties of the nanotube.

In this work, we use electronic structure calculations based on density functional theory (DFT) to investigate the interplay between TDs and excitons in (6,5) SWCNTs, which valuable for the use of semiconducting SWCNTs in optoelectronic devices. We explore how the presence of TDs affects the localization of unpaired electrons in the triplet states of excitons and calculate their ZFS parameters. Subsequently, we demonstrate that the most favorable of the studied TDs exhibits properties of a feasible single-photon emitter.

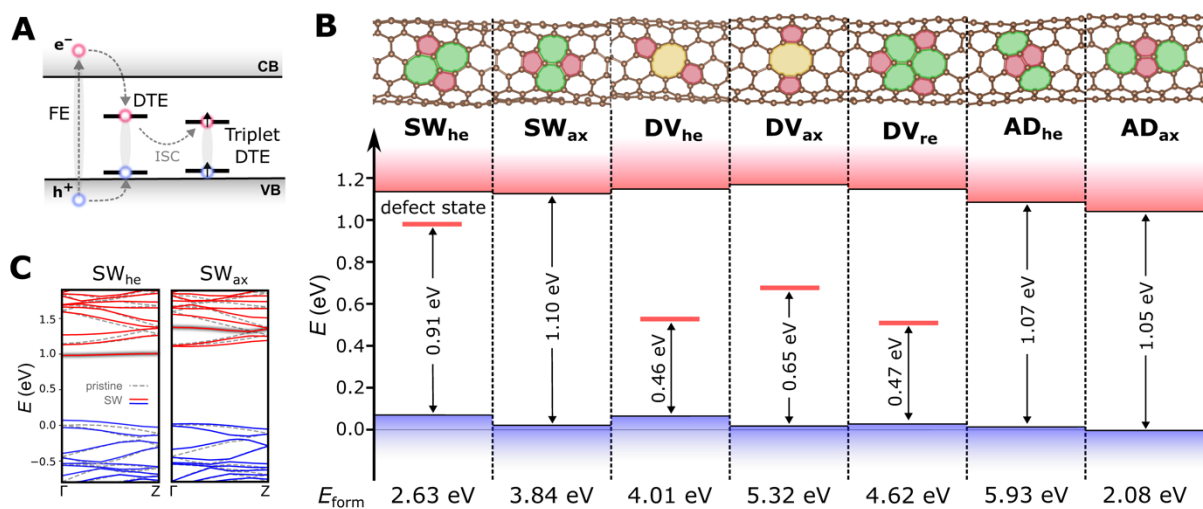


Figure 1. (A) Schematic depiction of the formation of a free exciton (FE), a defect-trapped exciton (DTE), and a triplet DTE. (B) Sketch of the atomic structures of the modelled topological defects in the (6,5) SWCNT (*top*) and the corresponding Kohn-Sham states at the Γ -point. Defect-induced unoccupied states in the band gap are depicted as solid red lines. In case of SW_{ax} , AD_{he} , and AD_{ax} , these states are situated in the conduction band. For all cases, the energy gap between the highest occupied and lowest unoccupied states are marked with vertical arrows. The zero energy is set at the VB maximum of pristine (6,5) SWCNT. (c) Calculated band structures of the SWCNT containing SW_{he} and SW_{ax} (solid lines; blue = occupied, red = unoccupied) superimposed with that of the pristine (6,5) nanotube (dashed lines). Localized defect states are highlighted with dark grey shading.

We begin our analysis by modeling the (6,5) SWCNT containing the TDs in their singlet ground state. The DFT calculations were carried out using a supercell model with periodic boundary conditions using the Quantum ESPRESSO program [32, 33]. The supercell contained 364 carbon atoms, corresponding to approximately a 4.07 nm segment of the nanotube. In both lateral dimensions, the nanotube in the supercell was surrounded by 16 Å of vacuum. Structural relaxation was performed at the gamma point, using the plane-wave energy cutoff of 40 Ry and the PBE exchange-correlation functional [34]. Subsequently, the HSE06 [35] hybrid functional was utilized for electronic structure and ZFS calculations.

The studied TDs are depicted in Figure 1B. All these defects can be introduced into the SWCNT at the cost of local distortion without the global chirality change (unlike, for example, a simple 5-7 pair [36]). Aside from two SWs with different orientations relative to the SWCNT axis (*helical*, SW_{he} , and *axial*, SW_{ax}), we considered another common TD—divacancies (DV_{he} and DV_{ax}) formed by the removal of two adjacent carbon atoms, resulting in the structure comprised of one octagon and two pentagons (5-8-5) [37]. Since this DV configuration is fully reconstructed to form an sp^2 -hybridized system, it does not contain dangling bonds (in contrast to a single vacancy). Additionally, the divacancy defect in graphene is reported to spontaneously transform into a stable defect structure consisting of three pentagon and three heptagon rings [38]. We consider this reconstructed divacancy and label it DV_{re} .

We also modeled another noteworthy type of TD formed by the adsorption of a carbon dimer [39, 40]. Unlike single adatoms, a dimer can incorporate as a part of the sp^2 -hybridized carbon system and therefore can be regarded as a TD. The resulting ad-dimer TD (denoted as AD_{he} and AD_{ax} in Figure 1B) comprises two pentagons and two heptagons (7-5-5-7) and is often referred to as a Stone-Wales defect [41].

First, we calculated the formation energies of the TDs as $E_{form} = E_{defect} - E_p + n\mu$, where E_{defect} and E_p are total energy of defect-containing and pristine supercells, respectively, μ is the chemical potential of carbon estimated as the total energy per atom in pristine nanotube, and n is number of removed/added carbon atoms ($n = 0$ for SW, 2 for DV, and -2 for AD). The calculated formation energies are listed in Figure 1B and range from 2 to 6 eV, in qualitative agreement with values reported for similar defects in graphene [42, 43]. Our results suggest SW_{he} and AD_{ax} as the most energetically favorable TDs among those considered. There is also a notable difference in the E_{form} values between axial and helical configurations of each TD, which is expected due to induced local deformations and differences in strain distribution patterns.

Next, we analyzed how each TD affects the electronic structure of the SWCNT. The Kohn-Sham states corresponding to the valence band (VB) maximum and conduction band (CB) minimum for defect-containing supercells are depicted in Figure 1B. The incorporation of TDs perturbs the VB and CB states, leading to a slight decrease in the band gap compared to the pristine (6,5) SWCNT, which is 1.15 eV in our DFT calculations. Notably, the SW_{he} defect introduces an additional unoccupied state into the band gap, situated close to the CB minimum (0.15 eV below). When an electron is excited from the VB to the CB (e.g., through photoexcitation), it is likely to fall into this shallow trap (cf. Figure 1A). Similarly, each divacancy features one clearly distinguishable empty defect level in the band gap. However, unlike the shallow trap introduced by SW_{he} , divacancy defect states are classified as deep

(mid-gap) traps, lying far from the band edges. These deep traps typically act as efficient recombination centers. An electron trapped in a mid-gap state can recombine with a hole from the VB, and vice versa [44, 45].

We then examined the band structure of the two SW defect configurations in more detail (Figure 1C). Despite representing the same defect type, they have strikingly different manifestation in the band structure of the SWCNT. In contrast to SW_{he} , the supercell containing SW_{ax} does not exhibit unoccupied states in the band gap. However, the inspection of CB reveals a localized defect-induced state with nearly flat dispersion about 0.3 eV from the CB minimum, which may stabilize upon trapping a photoexcited electron.

Another prominent difference between SW_{he} and SW_{ax} is their effect on the VB maximum. In the pristine (6,5) SWCNT, the VB maximum at the Γ -point comprises two degenerate states (see dashed lines in Figure 1C). These states have similar electron density distributions, delocalized over the entire nanotube [14]. Introducing TDs lifts this degeneracy. In the case of SW_{ax} , the resulting splitting at the Γ -point is relatively subtle, below 0.03 eV. In contrast, the effect is substantial in the supercell containing the SW_{he} defect. While one of the former VB maximum states largely retains its character and delocalization, the other shifts up into the band gap by about 0.1 eV and becomes significantly localized around the TD.

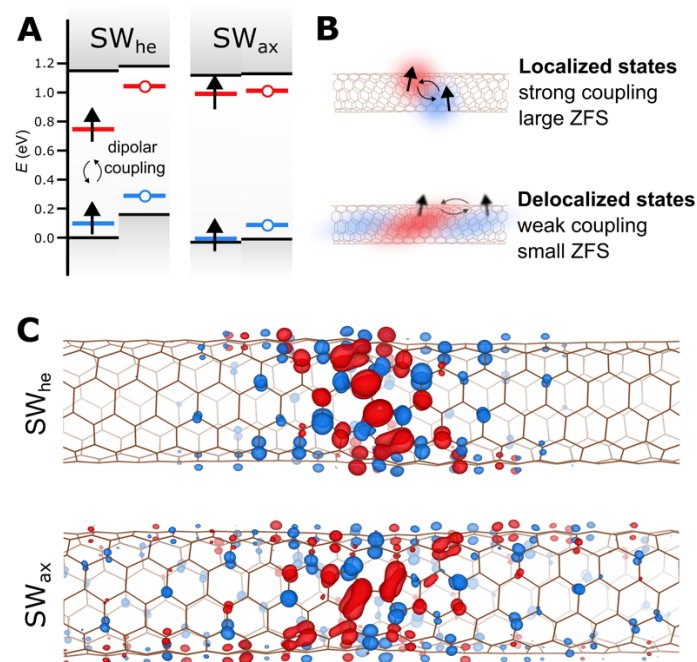


Figure 2. (A) Schematic diagram of the DFT calculated electronic structure of the triplet ($S = 1$; DTE) states of SW_{he} (left) and SW_{ax} (right). (B) A sketch illustrating the relation between delocalization between unpaired electron and the magnitude of ZFS. (C) Partial charge density contours of the two unpaired electrons (“hole” – blue, “electron” – red) for the SW triplet DTEs. Since the unpaired electrons of SW_{ax} are resonant with the CB and VB, they are substantially more delocalized compared to those of SW_{he} .

As a result, triplet excitons trapped at the SW_{he} and SW_{ax} defects exhibit substantially different electron density distributions. We modeled the triplet states by constraining the

total magnetization of the supercell. As shown in Figure 2A, one of the unpaired electrons of SW_{he} is expectedly stabilized at the formerly unoccupied in-gap defect level and the other one resides at the defect-centered VB maximum state. In the case of SW_{ax} , one unpaired electron occupies a state resonant with the valence band, resulting in substantial delocalization.

Electron density localization directly affects the magnitudes of their ZFS (as shown in Figure 2B). In light-element systems such as SWCNTs, the ZFS is primarily caused by the anisotropic magnetic dipole-dipole interaction between the unpaired electrons involved in the triplet state. This interaction decreases with the cube of the distance between the electrons (r^{-3}). Therefore, when the electron density is spread out, the average distance between the electrons increases, reducing the ZFS. Conversely, in triplet systems where the electrons are confined to a small region, their distance is smaller on average, leading to stronger dipole-dipole interactions and larger ZFS parameters.

In this work, we calculate the full dipole-dipole induced ZFS tensors from the Kohn-Sham electron densities using our recently developed computational approach [46, 47]. Conventionally, we describe ZFS by two parameters, D and E , according to the following spin Hamiltonian: $H_{ZFS} = D(S_z^2 - \frac{1}{3}S(S+1)) + E(S_x^2 - S_y^2)$, where S_x , S_y , and S_z are the effective spin operators. Figure 2C illustrates that in the triplet state of SW_{he} , one of the unpaired electrons is stabilized at the formerly unoccupied mid-gap level and the other resides at the defect-centered VB maximum state (cf. Figure 2A). Consequently, both of their electron densities are well-localized around the defect site, leading to a relatively large D value of -473.06 MHz (-1.95 μ eV; see Table 1), in good agreement with the experimentally observed triplet in (6,5) SWCNT ($D = |345|$ MHz in Ref. [25]; $D = |550|$ MHz in Ref. [27]).

While the sign of D cannot be determined from the reported ODMR measurements, our calculations for SW_{he} , which show $D < 0$, indicate that the spin density is stretched along the nanotube axis. The calculated angle between the axis and the principal direction of D is only about 3° . At the same time, our calculations reveal significant deviation of the spin density distribution from axial symmetry, which influences the anisotropy of the dipole-dipole interaction expressed as the ZFS parameter E . Our calculated E/D ratio of 0.26 suggests strong azimuthal anisotropy (rhombicity), which agrees with $E/D = 0.23$ derived from the experimental ODMR data in Ref. [25].

In contrast to the SW_{he} case, SW_{ax} is an example of a system where one of the electrons constituting the triplet resides on the state resonant with the valence band. This state largely retains the character of the VB maximum of a pristine nanotube, resulting in substantial delocalization (cf. Figure 2A,B). The situation where one electron is relatively confined, and the other is spread over the SWCNT direction manifests in a considerably smaller D value around -100 MHz directed along the nanotube axis.

Similarly, we compute the D and E values for the triplet states of all other TDs considered in this work (namely, DVs and ADs). The results are listed in Table 1. A noteworthy entry is DV_{re} , with its high spin density localization and large ZFS comparable to that of SW_{he} . However, since this defect features a deep mid-gap state and relatively high formation energy, we still consider SW_{he} as the most likely candidate for the experimentally observed triplet exciton. As for the rest of the defects, they exhibit D value in the range of 100-200 MHz and thus can be

candidates for the triplet exciton with $D = |150|$ MHz detected in Ref. [27]. The important conclusion of our result is that even a relatively small D value of 100-200 MHz implies substantial localization of the spin density, unlikely to be achieved in pristine nanotubes [49].

Table 1. DFT-calculated spin-spin ZFS (D and E values along with the angle θ between the D principal direction and the nanotube axis) of triplet excitons trapped by TDs.

Defect	D , MHz*	E , MHz	θ , deg
SW_{he}	-473.06	-123.58	3.13
SW_{ax}	-100.81	-25.49	7.86
DV_{he}	89.90	3.68	16.18
DV_{ax}	-197.97	-6.59	25.42
DV_{re}	307.72	58.44	95.33
AD_{he}	-136.07	-1.26	7.56
AD_{ax}	-107.89	23.89	91.85

*For comparison, the D values obtained from the experimental ODMR spectra in Ref. [27] are $|550|$ MHz and $|150|$ MHz for the excitons labeled T1 and T2, respectively. In Ref. [25], the experimental ODMR spectra were simulated with $D = |345|$ MHz and $E = |78|$ MHz.

After identifying SW_{he} as the most likely exciton trapping site, we aim to study its lowest singlet excited state (labeled S_0 in Figure 3A). Since both its highest occupied and lowest unoccupied levels (the defect-centered VB maximum and the shallow trap state, respectively) reside in the band gap, the excited singlet S_0 is likely associated with the internal transition between these two levels. To model this internal transition of SW_{he} , we employ the Δ SCF approach [50], in which the excited singlet S_1 is simulated by imposing constrained occupations of the Kohn-Sham states with subsequent atomic relaxation. Subsequently, we compute configuration coordinate diagrams to schematically depict the coupling of the $S_0 \leftrightarrow S_1$ transition to lattice vibrations. The effective one-dimensional configuration coordinate Q is defined according to the approach introduced by Alkauskas et al. [45, 51].

The calculated zero-phonon line (ZPL) for the $S_0 \leftrightarrow S_1$ transition is 0.77 eV (1610 nm), suggesting that the SW_{he} TD is likely to emit in the telecom L-band. The structural change, ΔQ , between the ground and excited states is moderate, constituting $0.37 \text{ amu}^{1/2}\text{\AA}$ (amu = atomic mass units). Subsequently, we determine the Huang-Rhys factor within the one-dimensional approximation as $S_{HR} = \frac{1}{2\hbar}\Omega\Delta Q^2$, where Ω is the effective frequency [51, 52]. The computed Huang-Rhys factor is only 0.74, signifying weak electron-phonon coupling and a low number of phonons involved in the transition. Therefore, defects with a low Huang-Rhys factor ($S_{HR} \approx 1$) exhibit a high fraction of photons emitted into the ZPL. These photons are in a well-defined quantum state and are thus useful for quantum information applications [53]. Consequently, our calculations suggest that the SW_{he} defect in (6,5) SWCNT demonstrates the features of a promising L-band single-photon emitter.

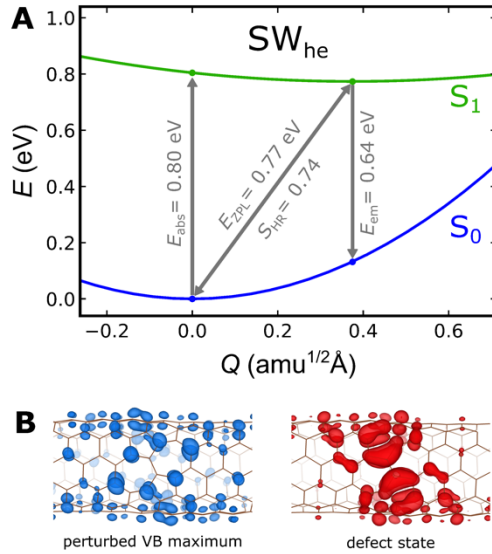


Figure 3. (A) Configuration coordinate diagram of the $S_0 \rightarrow S_1$ internal transition of the SW_{he} defect in (6,5) SWCNT obtained from DFT calculations. The grey lines indicate optical transitions, labeled with the corresponding transition energies (E_{abs} , E_{em} , and E_{ZPL} stand for absorption, emission, and zero-phonon line, respectively). (B) Charge density isosurface of the two states involved in the $S_0 \rightarrow S_1$ transition: the perturbed VB maximum that is occupied in the ground state S_0 (left) and the defect-induced trap state that becomes occupied in the excited state S_1 (right).

Another remarkable result of our ΔSCF calculations for SW_{he} is a vanishing energy gap between S_1 and the excited triplet state (commonly termed the singlet–triplet gap, $\Delta E_{ST} = 0.004$ eV in our calculations). Small ΔE_{ST} signifies minimal spatial overlap between the orbitals involved in the formation of the S_1 state, which minimizes the exchange integral [54, 55]. As illustrated in Figure 3B, a minimal exchange integral is achieved by the localization of the electron densities on alternating atoms of the SW_{he} system. Organic molecules with similar properties are often designed to act as chromophores for organic light-emitting diodes [56], where a reduced singlet–triplet gap is desirable as it facilitates efficient thermally activated delayed fluorescence (TADF) via reverse ISC from the triplet state to S_1 .

In summary, our computational results provide valuable insights into the photophysics of topological defects in semiconducting SWCNTs. The TDs considered in this work only introduce local distortions and do not affect the chirality, making their presence inconsequential to many experimental observations [29]. However, they can make significant impact on the electronic structure of the nanotube and, accordingly, on exciton dynamics. Our data show that TDs provide sufficient electron density localization of the triplet excitonic state to achieve the experimentally observed range of ZFS values. Among the studied TDs, SW_{he} exhibits particularly intriguing properties. This defect introduces a shallow trap state into the band gap and causes electron density localization at the valence band maximum. As a result, the unpaired electrons involved in its triplet state are spatially confined, leading to a relatively large ZFS and rendering it a plausible defect to be associated with the triplet exciton observed in Refs. [24, 25, 27]. Notably, the lowest singlet excited state of SW_{he} can undergo a radiative internal transition to the ground state with a ZPL at 1610 nm (in the telecom L-band) and a low Huang-Rhys factor of 0.74, providing compelling possibilities for applications as single-photon emitters.

ACKNOWLEDGEMENTS

We are grateful to Sofie Cambré and Etienne Goovaerts for helpful discussions. We acknowledge Deutsche Forschungsgemeinschaft (DFG) from TRR 332 142/3-2024, Project No. 231447078 for funding as well as the Paderborn Center for Parallel Computing (PC2) for the provided computational resources.

REFERENCES

1. Dresselhaus, G.; Dresselhaus, M. S.; Saito, R. *Physical Properties of Carbon Nanotubes*; World Scientific, 1998.
2. Dong, Z.; Li, W.; Wang, H.; Jiang, X.; Liu, H.; Zhu, L.; Chen, H. Carbon Nanotubes in Perovskite-Based Optoelectronic Devices. *Matter* **2022**, *5* (2), 448-481. DOI: 10.1016/j.matt.2021.12.011
3. Blackburn, J. L. Semiconducting Single-Walled Carbon Nanotubes in Solar Energy Harvesting. *ACS Energy Lett.* **2017**, *2* (7), 1598-1613. DOI: 10.1021/acsenergylett.7b00228
4. Avouris, P.; Freitag, M.; Perebeinos, V. Carbon-Nanotube Photonics and Optoelectronics. *Nat. Photonics* **2008**, *2* (6), 341-350. DOI: 10.1038/nphoton.2008.94
5. Ghosh, S.; Bachilo, S. M.; Simonette, R. A.; Beckingham, K. M.; Weisman, R. B. Oxygen Doping Modifies Near-Infrared Band Gaps in Fluorescent Single-Walled Carbon Nanotubes. *Science* **2010**, *330*, 1656-1659. DOI: 10.1126/science.1196382
6. Diao, S.; Blackburn, J. L.; Hong, G.; Antaris, A. L.; Chang, J.; Wu, J. Z.; Zhang, B.; Cheng, K.; Kuo, C. J.; Dai, H. Fluorescence Imaging in Vivo at Wavelengths Beyond 1500 nm. *Angew. Chem.* **2015**, *127* (49), 14971-14975. DOI: 10.1002/ange.201507473
7. He, X.; Htoon, H.; Doorn, S. K.; Pernice, W. H.; Pyatkov, F.; Krupke, R.; Jeantet, A.; Chassagneux, Y.; Voisin, C. Carbon Nanotubes as Emerging Quantum-Light Sources. *Nat. Mater.* **2018**, *17*, 663-670. DOI: 10.1038/s41563-018-0109-2
8. Jeantet, A.; Chassagneux, Y.; Raynaud, C.; Roussignol, P.; Lauret, J. S.; Besga, B.; Estève, J.; Reichel, J.; Voisin, C. Widely Tunable Single-Photon Source from a Carbon Nanotube in the Purcell Regime. *Phys. Rev. Lett.* **2016**, *116*, 247402. DOI: 10.1103/PhysRevLett.116.247402
9. Khasminskaya, S.; Pyatkov, F.; Słowik, K.; Ferrari, S.; Kahl, O.; Kovalyuk, V.; Rath, P.; Vetter, A.; Henrich, F.; Kappes, M. M.; Gol'Tsman, G. Fully Integrated Quantum Photonic Circuit with an Electrically Driven Light Source. *Nat. Photonics* **2016**, *10* (11), 727-732. DOI: 10.1038/nphoton.2016.178
10. Wei, X.; Li, S.; Wang, W.; Zhang, X.; Zhou, W.; Xie, S.; Liu, H. Recent advances in structure separation of single-wall carbon nanotubes and their application in optics, electronics, and optoelectronics. *Adv. Science.* **2022**, *9*, 2200054. DOI: 10.1002/advs.202200054
11. Janas, D. Towards Monochiral Carbon Nanotubes: A Review of Progress in the Sorting of Single-Walled Carbon Nanotubes. *Mater. Chem. Front.* **2018**, *2* (1), 36-63. DOI: 10.1039/C7QM00427C
12. Maultzsch, J.; Pomraenke, R.; Reich, S.; Chang, E.; Prezzi, D.; Ruini, A.; Molinari, E.; Strano, M. S.; Thomsen, C.; Lienau, C. Large Binding Energies in Excitons of Single-Walled Carbon Nanotubes. *Phys. Rev. B* **2005**, *72*, 241402. DOI: 10.1103/PhysRevB.72.241402
13. Hertel, T.; Himmelein, S.; Ackermann, T.; Stich, D.; Crochet, J. Diffusion Limited Photoluminescence Quantum Yields in 1-D Semiconductors: Single-Wall Carbon Nanotubes. *ACS Nano* **2010**, *4* (12), 7161-7168. DOI: 10.1021/nn101612b
14. Gifford, B. J.; Kilina, S.; Htoon, H.; Doorn, S. K.; Tretiak, S. Controlling Defect-State Photophysics in Covalently Functionalized Single-Walled Carbon Nanotubes. *Acc. Chem. Res.* **2020**, *53* (9), 1791-1801. DOI: 10.1021/acs.accounts.0c00210
15. Zaumseil, J. Luminescent Defects in Single-Walled Carbon Nanotubes for Applications. *Adv. Opt. Mater.* **2022**, *10* (2), 2101576. DOI: 10.1002/adom.202101576
16. Luo, Y.; He, X.; Kim, Y.; Blackburn, J. L.; Doorn, S. K.; Htoon, H.; Strauf, S. Carbon Nanotube Color Centers in Plasmonic Nanocavities: A Path to Photon Indistinguishability at Telecom Bands. *Nano Lett.* **2019**, *19* (12), 9037-9044. DOI: 10.1021/acs.nanolett.9b04069
17. He, X.; Hartmann, N. F.; Ma, X.; Kim, Y.; Ihly, R.; Blackburn, J. L.; Gao, W.; Kono, J.; Yomogida, Y.; Hirano, A.; Tanaka, T. Tunable Room-Temperature Single-Photon Emission at Telecom Wavelengths from sp^3 Defects in Carbon Nanotubes. *Nat. Photonics* **2017**, *11* (9), 577-582. DOI: 10.1038/nphoton.2017.119

18. Ma, X.; Hartmann, N. F.; Baldwin, J. K.; Doorn, S. K.; Htoon, H. Room-Temperature Single-Photon Generation from Solitary Dopants of Carbon Nanotubes. *Nat. Nanotechnol.* **2015**, *10* (8), 671-675. DOI: 10.1038/nnano.2015.136
19. Kasha, M. Characterization of Electronic Transitions in Complex Molecules. *Discuss. Faraday Soc.* **1950**, *9*, 14-19. DOI: 10.1039/DF9500900014
20. Kim, K. H.; Yoo, S. J.; Kim, J. J. Boosting Triplet Harvest by Reducing Nonradiative Transition of Exciplex Toward Fluorescent Organic Light-Emitting Diodes with 100% Internal Quantum Efficiency. *Chem. Mater.* **2016**, *28* (6), 1936-1941. DOI: 10.1021/acs.chemmater.6b00478
21. Mayländer, M.; Thielert, P.; Quintes, T.; Vargas Jentzsch, A.; Richert, S. Room Temperature Electron Spin Coherence in Photogenerated Molecular Spin Qubit Candidates. *J. Am. Chem. Soc.* **2023**, *145* (25), 14064-14069. DOI: 10.1021/jacs.3c04021
22. Fukuda, R.; Umeyama, T.; Tsujimoto, M.; Ishidate, F.; Tanaka, T.; Kataura, H.; Imahori, H.; Murakami, T. Sustained Photodynamic Effect of Single Chirality-Enriched Single-Walled Carbon Nanotubes. *Carbon* **2020**, *161*, 718-725. DOI: 10.1016/j.carbon.2020.02.002
23. Park, J.; Deria, P.; Therien, M. J. Dynamics and Transient Absorption Spectral Signatures of the Single-Wall Carbon Nanotube Electronically Excited Triplet State. *J. Am. Chem. Soc.* **2011**, *133* (43), 17156-17159. DOI: 10.1021/ja2079477
24. Stich, D.; Späth, F.; Kraus, H.; Sperlich, A.; Dyakonov, V.; Hertel, T. Triplet-Triplet Exciton Dynamics in Single-Walled Carbon Nanotubes. *Nat. Photonics* **2014**, *8* (2), 139-144. DOI: 10.1038/nphoton.2013.316
25. Kraus, H. *Optically detected magnetic resonance on organic and inorganic carbon-based semiconductors*; Doctoral dissertation, Universität Würzburg, 2014.
26. Palotás, J.; Negyedi, M.; Kollarics, S.; Bojtor, A.; Rohringer, P.; Pichler, T.; Simon, F. Incidence of Quantum Confinement on Dark Triplet Excitons in Carbon Nanotubes. *ACS Nano* **2020**, *14* (9), 11254-11261. DOI: 10.1021/acsnano.0c03139
27. Sudakov, I.; Goovaerts, E.; Wenseleers, W.; Blackburn, J. L.; Duque, J. G.; Cambré, S. Chirality Dependence of Triplet Excitons in (6, 5) and (7, 5) Single-Wall Carbon Nanotubes Revealed by Optically Detected Magnetic Resonance. *ACS Nano* **2023**, *17* (3), 2190-2204. DOI: 10.1021/acsnano.2c08392
28. Abragam, A.; Bleaney, B. *Electron Paramagnetic Resonance of Transition Ions*; Oxford University Press, 2012.
29. Collins, P. G. *Defects and Disorder in Carbon Nanotubes*; Oxford University Press, 2010.
30. Yuan, Q.; Xu, Z.; Yakobson, B. I.; Ding, F. Efficient Defect Healing in Catalytic Carbon Nanotube Growth. *Phys. Rev. Lett.* **2012**, *108* (24), 245505. DOI: 10.1103/PhysRevLett.108.245505
31. Ertekin, E.; Chrzan, D. C.; Daw, M. S. Topological description of the Stone-Wales defect formation energy in carbon nanotubes and graphene. *Phys. Rev. B* **2009**, *79* (15), 155421. DOI: 10.1103/PhysRevB.79.155421
32. Gianozzi, P. et al. QUANTUM ESPRESSO: A Modular and Open-Source Software Project for Quantum Simulations of Materials. *J. Phys.: Condens. Matter* **2009**, *21*, 395502. DOI: 10.1088/0953-8984/21/39/395502
33. Gianozzi, P. et al. Advanced Capabilities for Materials Modeling with Quantum ESPRESSO. *J. Chem. Phys.* **2017**, *29*, 465901. DOI: 10.1088/1361-648X/aa8f79
34. Perdew, J. P.; Burke, K.; Ernzerhof, M. Generalized Gradient Approximation Made Simple. *Phys. Rev. Lett.* **1996**, *77*, 3865. DOI: 10.1103/PhysRevLett.77.3865
35. Heyd, J.; Scuseria, G. E.; Ernzerhof, M. Hybrid Functionals Based on a Screened Coulomb Potential. *J. Chem. Phys.* **2003**, *118*, 8207-8215. DOI: 10.1063/1.1564060
36. Chico, L.; Benedict, L. X.; Louie, S. G.; Cohen, M. L. Quantum Conductance of Carbon Nanotubes with Defects. *Phys. Rev. B* **1996**, *54* (4), 2600. DOI: 10.1103/PhysRevB.54.2600
37. Kotakoski, J.; Krasheninnikov, A. V.; Nordlund, K. Structure of Divacancies in Carbon Nanotubes. *Phys. Rev. B* **2006**, *74*, 245420. DOI: 10.1103/PhysRevB.74.245420
38. Lee, G. D.; Wang, C. Z.; Yoon, E.; Hwang, N. M.; Kim, D. Y.; Ho, K. M. Diffusion, Coalescence, and Reconstruction of Vacancy Defects in Graphene Layers. *Phys. Rev. Lett.* **2005**, *95* (20), 205501. DOI: 10.1103/PhysRevLett.95.205501
39. Sternberg, M.; Curtiss, L. A.; Gruen, D. M.; Kedziora, G.; Horner, D. A.; Redfern, P. C.; Zapol, P. Carbon Ad-Dimer Defects in Carbon Nanotubes. *Phys. Rev. Lett.* **2006**, *96* (7), 075506. DOI: 10.1103/PhysRevLett.96.075506
40. Orlikowski, D.; Nardelli, M. B.; Bernholc, J.; Roland, C. Carbon Dimers on Graphene. *Phys. Rev. Lett.* **1999**, *83*, 4132. DOI: 10.1103/PhysRevLett.83.4132

41. Lusk, M. T.; Carr, L. D. Nanoengineering Defect Structures on Graphene. *Phys. Rev. Lett.* **2008**, *100*, 17550. DOI: 10.1103/PhysRevLett.100.175503
42. Skowron, S. T.; Lebedeva, I. V.; Popov, A. M.; Bichoutskaia, E. Energetics of Atomic Scale Structure Changes in Graphene. *Chem. Soc. Rev.* **2015**, *44* (10), 3143-3176. DOI: 10.1039/C4CS00499J
43. Banhart, F.; Kotakoski, J.; Krasheninnikov, A. V. Structural Defects in Graphene. *ACS Nano* **2011**, *5* (1), 26-41. DOI: 10.1021/nn102598m
44. Shockley, W. T.; Read, W. T., Jr. Statistics of the Recombination of Holes and Electrons. *Phys. Rev.* **1952**, *87* (5), 835. DOI: 10.1103/PhysRev.87.835
45. Alkauskas, A.; Yan, Q.; Van de Walle, C. G. First-Principles Theory of Nonradiative Carrier Capture via Multiphonon Emission. *Phys. Rev. B* **2014**, *90* (7), 075202. DOI: 10.1103/PhysRevB.90.075202
46. Biktagirov, T.; Schmidt, W. G.; Gerstmann, U. Calculation of Spin-Spin Zero-Field Splitting within Periodic Boundary Conditions: Towards All-Electron Accuracy. *Phys. Rev. B* **2018**, *97* (11), 115135. DOI: 10.1103/PhysRevB.97.115135
47. Biktagirov, T.; Schmidt, W. G.; Gerstmann, U. Spin Decontamination for Magnetic Dipolar Coupling Calculations: Application to High-Spin Molecules and Solid-State Spin Qubits. *Phys. Rev. Res.* **2020**, *2* (2), 022024. DOI: 10.1103/PhysRevResearch.2.022024
48. Richert, S.; Tait, C. E.; Timmel, C. R. Delocalisation of Photoexcited Triplet States Probed by Transient EPR and Hyperfine Spectroscopy. *J. Magn. Reson.* **2017**, *280*, 103-116. DOI: 10.1016/j.jmr.2017.01.005
49. Mann, C.; Hertel, T. 13 nm Exciton Size in (6, 5) Single-Wall Carbon Nanotubes. *J. Phys. Chem. Lett.* **2016**, *7* (12), 2276-2280. DOI: 10.1021/acs.jpcllett.6b00797
50. Jones, R. O.; Gunnarsson, O. The Density Functional Formalism, Its Applications and Prospects. *Rev. Mod. Phys.* **1989**, *61* (3), 689. DOI: 10.1103/RevModPhys.61.689
51. Alkauskas, A.; Lyons, J. L.; Steiauf, D.; Van de Walle, C. G. First-Principles Calculations of Luminescence Spectrum Line Shapes for Defects in Semiconductors: The Example of GaN and ZnO. *Phys. Rev. Lett.* **2012**, *109* (26), 267401. DOI: 10.1103/PhysRevLett.109.267401
52. Schanovsky, F.; Gös, W.; Grasser, T. Multiphonon Hole Trapping from First Principles. *J. Vac. Sci. Technol. B* **2011**, *29* (1), 01A201. DOI: 10.1116/1.3533269
53. Turiansky, M. E.; Parto, K.; Moody, G.; Van de Walle, C. G. Rational Design of Efficient Defect-Based Quantum Emitters. *arXiv* **2024**, *2402*, 08257
54. Chen, T.; Zheng, L.; Yuan, J.; An, Z.; Chen, R.; Tao, Y.; Li, H.; Xie, X.; Huang, W. Understanding the Control of Singlet-Triplet Splitting for Organic Exciton Manipulating: A Combined Theoretical and Experimental Approach. *Sci. Rep.* **2015**, *5*, 10923. DOI: 10.1038/srep10923
55. Milián-Medina, B.; Gierschner, J. Computational Design of Low Singlet-Triplet Gap All-Organic Molecules for OLED Application. *Org. Electron.* **2012**, *13* (6), 985-991. DOI: 10.1016/j.orgel.2012.02.010
56. Aizawa, N.; Pu, Y. J.; Harabuchi, Y.; Nihonyanagi, A.; Ibuka, R.; Inuzuka, H.; Dhara, B.; Koyama, Y.; Nakayama, K. I.; Maeda, S.; Araoka, F. Delayed Fluorescence from Inverted Singlet and Triplet Excited States. *Nature* **2022**, *609*, 502-506. DOI: 10.1038/s41586-022-05132-y